Clinical Cancer Research

Macropinocytosis of Bevacizumab by Glioblastoma Cells in the Perivascular Niche Affects their Survival

Gaëlle Müller-Greven[1,2], Cathleen R. Carlin[3], Monica E. Burgett[1,2], Manmeet S. Ahluwalia[4], Adam Lauko[1], Amy S. Nowacki[5], Cameron J. Herting[6], Maha A. Qadan[1,2], Markus Bredel[7], Steven A. Toms[8], Justin D. Lathia[4,9], Dolores Hambardzumyan[6], Jann N. Sarkaria[10], Petra Hamerlik[11], and Candece L. Gladson[1,4]

Abstract

Purpose: Bevacizumab, a humanized monoclonal antibody to VEGF, is used routinely in the treatment of patients with recurrent glioblastoma (GBM). However, very little is known regarding the effects of bevacizumab on the cells in the perivascular space in tumors.

Experimental Design: Established orthotopic xenograft and syngeneic models of GBM were used to determine entry of monoclonal anti-VEGF-A into, and uptake by cells in, the perivascular space. Based on the results, we examined $CD133^+$ cells derived from GBM tumors *in vitro*. Bevacizumab internalization, trafficking, and effects on cell survival were analyzed using multilabel confocal microscopy, immunoblotting, and cytotoxicity assays in the presence/absence of inhibitors.

Results: In the GBM mouse models, administered anti-mouse-VEGF-A entered the perivascular tumor niche and was internalized by $Sox2^+/CD44^+$ tumor cells. In the perivascular tumor cells, bevacizumab was detected in the recycling compartment or the lysosomes, and increased autophagy was found. Bevacizumab was internalized rapidly by $CD133^+/Sox2^+$-GBM cells *in vitro* through macropinocytosis with a fraction being trafficked to a recycling compartment, independent of FcRn, and a fraction to lysosomes. Bevacizumab treatment of $CD133^+$ GBM cells depleted VEGF-A and induced autophagy thereby improving cell survival. An inhibitor of lysosomal acidification decreased bevacizumab-induced autophagy and increased cell death. Inhibition of macropinocytosis increased cell death, suggesting macropinocytosis of bevacizumab promotes $CD133^+$ cell survival.

Conclusions: We demonstrate that bevacizumab is internalized by $Sox2^+/CD44^+$-GBM tumor cells residing in the perivascular tumor niche. Macropinocytosis of bevacizumab and trafficking to the lysosomes promotes $CD133^+$ cell survival, as does the autophagy induced by bevacizumab depletion of VEGF-A. *Clin Cancer Res; 23(22); 7059–71. ©2017 AACR.*

Introduction

The microenvironment provided in the perivascular space is emerging as a critical determinant of tumor cell growth and survival (reviewed in ref. 1). Although humanized IgG mAbs are now used in cancer therapy, surprisingly little is known concerning their access to the perivascular space in the brain and the mechanisms by which they affect tumor cells within this microenvironment. Bevacizumab, a humanized bivalent IgG1 mAb, was developed as an anti-angiogenic therapeutic agent. Currently, bevacizumab has FDA approval for use in the treatment of recurrent glioblastoma (GBM) and renal, lung, and colon cancer (2). Bevacizumab has been reported to extend the 6-month progression-free survival in patients with recurrent GBM (3, 4). Patients with recurrent GBM are now routinely treated with bevacizumab, which induces normalization of some of the tumor vasculature (2) and enhances quality-of-life. In common with other humanized mAbs, the response shows interindividual variability and approximately 20% of patients with recurrent GBM do not show any response to bevacizumab (5). The reasons for this lack of response have not been elucidated and the effects of bevacizumab on the cells in the perivascular niche have not been determined.

It is well established that populations of cells with a cancer stem cell-like phenotype (e.g., expression of the CD133 cell surface marker and of the transcription factor Sox2) are resistant to radiation therapy (6). Thus, alterations in the perivascular microenvironment could provide a niche that promotes and then

[1]Department of Cancer Biology, Cleveland Clinic, Cleveland, Ohio. [2]School of Biomedical Sciences, Kent State University, Kent, Ohio. [3]Department of Molecular Biology and Microbiology, Case Western Reserve University, Cleveland, Ohio. [4]Brain Tumor and Neuro-Oncology Center, Taussig Cancer Institute, Cleveland Clinic, Cleveland, Ohio. [5]Department of Quantitative Health Sciences, Cleveland Clinic, Cleveland, Ohio. [6]Department of Pediatrics, Emory University School of Medicine, Atlanta, Georgia. [7]Department of Radiation Oncology, University of Alabama at Birmingham, Birmingham, Alabama. [8]Department of Neurosurgery, Geisinger Medical Center, Geisinger, Pennsylvania. [9]Department of Cell and Molecular Medicine, Lerner Research Institute, Cleveland Clinic, Cleveland, Ohio. [10]Department of Radiation Oncology, Mayo Clinic, Rochester, Minnesota. [11]Brain Tumor Biology, Danish Cancer Society Research Center, Copenhagen, Denmark.

Note: Supplementary data for this article are available at Clinical Cancer Research Online (http://clincancerres.aacrjournals.org/).

Corresponding Author: Candece L. Gladson, Cleveland Clinic, 9500 Euclid Avenue, NB-40, Cleveland, OH 44195. Phone: 216-636-9493; Fax: 216-445-6269; E-mail: gladsoc@ccf.org

doi: 10.1158/1078-0432.CCR-17-0249

Translational Relevance

We found that bevacizumab is internalized by perivascular $Sox2^+/CD44^+$ tumor cells *in vivo* in orthotopic xenograft and syngeneic mouse models of glioblastoma. Bevacizumab was internalized by macropinocytosis in $CD133^+/Sox2^+$ tumor cells and when trafficked to the lysosome promoted tumor cell survival, as did the autophagy induced by bevacizumab depletion of VEGF-A. As we observed similar trafficking of bevacizumab and human IgG in $CD133^+$ tumor cells, these findings provide important insight into a new potential mechanism of resistance to bevacizumab or other monoclonal antibody therapies. Bevacizumab also is used to treat renal, colon, and lung cancer; thus, these studies may have applicability to other cancers.

sustains the development of this population of cells in various cancers, including GBM. Bevacizumab was developed based on its binding of vascular endothelial growth factor-A (VEGF-A) at the site recognized by the VEGF receptor (VEGFR) thereby preventing VEGF-A signaling (reviewed in ref. 2). As GBM cells with the $CD133^+$ phenotype produce VEGF-A and express VEGFR2, VEGF-A can act in an autocrine or paracrine manner to promote survival of these cells as well as acting systemically (7, 8).

Large molecules can gain access to the perivascular tissue through transcytosis across the endothelial cells (EC) in the brain, and through alterations in the blood–brain barrier (BBB; refs. 9, 10). Although it is a reasonable assumption that bevacizumab gains access to the perivascular space in GBM, to our knowledge there are no published reports demonstrating this. One report indicated that human IgG (hIgG) was detectable in tumor lysates of orthotopic GBM xenograft tumors that had been propagated in nude mice administered bevacizumab (11). However, this was based on Western blotting of whole tumor lysates and, thus, did not differentiate between the presence of the bevacizumab in the perivascular space and the tumor-associated vessels. Similarly, the possibility that bevacizumab is internalized by GBM tumor cells has not been addressed. Recently, fluorescent-labeled bevacizumab was shown to gain access to invasive breast cancers when injected intravenously prior to mastectomy (12). In ECs, hIgG is thought to be taken up by a pinocytotic process and to bind the embryonic Fc receptor (FcRn), which recycles hIgG and is localized at the early endosome (13, 14). FcRn is expressed in brain ECs (13, 14), but was found recently either to be undetectable or present at very low levels in a large number of tumor cell lines and that when present it acts as a tumor suppressor by recycling albumin (15). Large molecules also can be internalized through the nonselective process of macropinocytosis. Macropinocytosis is initiated from plasma membrane ruffles that give rise to actin-containing plasma membrane extensions, resulting in large endocytic vacuoles called macropinosomes that ultimately become early endosomes (reviewed in refs. 16, 17). The cargo within early endosomes can be trafficked to a recycling compartment or the lysosome (16, 17). Macropinocytosis has been shown to be a mechanism by which *Ras*-transformed cells and starving cells engulf extracellular proteins and then lysosomally degrade the proteins, thereby promoting their own proliferation and survival (18, 19).

Here, we report that bevacizumab and hIgG gain access to the perivascular space in orthotopic mouse models of GBM and that this access is associated with defects in the BBB rather than transcytosis across the tumor-associated vasculature. We found that perivascular $Sox2^+/CD44^+$ tumor cells are largely responsible for internalization of bevacizumab within the niche. In $CD133^+/Sox2^+$ cells, propagated in media without addition of growth factors, this internalization occurs through a mechanism consistent with macropinocytosis and that a fraction is localized to a "fast" recycling compartment independent of FcRn and another fraction is localized to the lysosome. The macropinocytosis of bevacizumab and its trafficking to the lysosome promotes survival of the $CD133^+$ cells, as does the autophagy induced by the bevacizumab-mediated depletion of VEGF-A.

Materials and Methods

Cells

Normal brain ECs (isolates 422 and 376) were purchased from Cell Systems; tumor-associated ECs (TEC) were isolated and propagated from primary human GBM tumors (20); $CD133^+$ cells and the matched (paired) $CD133^-$ (non-stem) tumor cells were isolated from two human GBM xenograft tumors (08-387 and 4121; ref. 21); and MM.1R human myeloma cells were purchased from the ATCC. Propagation of the cells and their authentication was as described in the Supplementary Methods.

Reagents

Described in the Supplementary Methods.

Expression of FcγRIIB in myeloma cells

FcγRIIB cDNA was purchased (EX-ZO435-Lv105, GeneCopoeia) and a lentivirus vector created and used to transduce MM.1R myeloma cells (22).

Animal studies

All studies were performed with the approval of the Animal Use and Care Committee of the Cleveland Clinic, Mayo Clinic or Emory University School of Medicine. The $CD133^+$ orthotopic GBM, the PDX orthotopic GBM, and the syngeneic somatic gene transfer GBM models were generated as described (21, 23, 24), with details provided in the Supplementary Methods. The $CD133^+$ and PDX models were established and treated with bevacizumab as described in the Supplemental Methods and Figure Legends. The somatic gene transfer model was generated and treated with rat anti-mouse-VEGF-A (25) as described in the Supplementary Methods and Figure Legends.

Immunofluorescence

$CD133^+$ GBM cells were plated overnight on chamber slides coated with 20 μg/mL laminin (R&D Systems #3400-00-01) in neural basal media (NBM) without addition of EGF or basic-FGF (bFGF). Maintenance of the stem-cell phenotype was verified by Sox2 expression (26, 27). The following day, a clinically relevant concentration (250 μg/mL; ref. 28) of bevacizumab was added to the media. After incubation (37°C, 5% CO_2) for 5 minutes, the cells were washed and fixed, or fresh media was added and the cells incubated for the times indicated. To detect internalized bevacizumab, cells were fixed with 4% buffered-paraformaldehyde, blocked, and reacted with Alexa Fluor 488-anti-human IgG, then mounted in media containing DAPI nuclear stain (Vector

Lab #280772). Double-label immunofluorescent analysis was performed as described previously (20, 29). Additional details are found in the Supplementary Methods.

Cytotoxicity assay

This assay was performed according to the manufacturer's instructions (CytoTox-Fluor Cytotoxicity Assay, Promega).

ELISA assays

VEGF-A, VEGF-C, and placental growth factor (PGF) were measured using VEGF-A&C (RayBiotech) and PGF (R&D-Systems) ELISA assay kits as recommended by the manufacturer.

Statistical analysis

All statistical analyses were performed or overseen by the biostatistician (ASN). The test used is stated in the Figure Legends. A P-value < 0.05 was considered significant.

Results

Bevacizumab gains access to the perivascular space and is internalized predominantly by perivascular Sox2$^+$/CD44$^+$ tumor cells in orthotopic xenograft and syngeneic mouse models of GBM

To determine whether bevacizumab can gain access to the perivascular space in GBM, we used a mouse model in which bevacizumab or a control hIgG was administered (i.v., 5 d) to mice with established GBM tumors. Bevacizumab and hIgG were detected in frozen sections of the brain by labeling with an Alexa Fluor 488-anti-human-IgG (green) and their location assessed by costaining with anti-von Willebrand factor (vWf), a marker of ECs, and Alexa Fluor 594-conjugated secondary antibody (red) together with nuclear staining using DAPI (blue). Both bevacizumab and the control hIgG were detectable in the perivascular space of the orthotopic GBM tumors (Supplementary Fig. S1A and S1B). Very little bevacizumab or hIgG was detected in the perivascular space of uninvolved brain from the mouse model (Supplementary Fig. S1A and S1B), consistent with prior studies indicating that minimal amounts of hIgG gain access to the perivascular tissue when the BBB is intact (30).

This analysis further indicated that bevacizumab is internalized by perivascular tumor cells in the GBM xenografts (Supplementary Fig. S1A and S1B). Using serial sections of xenograft tumors, we verified that the perivascular cells were human tumor cells by double-labeling with mAb anti-Sox2 and a rabbit antibody to human nuclei (Supplementary Fig. S1C). The relative distribution of bevacizumab in the Sox2$^+$ cells versus activated microglia/macrophages was determined using intracerebral GBM xenograft tumors obtained from mice in which the tumor was established and then bevacizumab administered until euthanasia. Sections of the tumors were stained with antibodies to Sox2 and Iba1 (27, 31), and the fluorescent intensity of bevacizumab quantified. Although both perivascular Sox2$^+$ cells and Iba1$^+$ cells internalized bevacizumab, the bevacizumab-intensity was ~2.5-fold higher in the perivascular Sox2$^+$ cells than perivascular Iba1$^+$ cells (Fig. 1A and B). On measuring the distance of Sox2$^+$ and Iba1$^+$ cells from the nearest blood vessel, we did not find a difference in proximity (Fig. 1C), consistent with the known localization of both cell types to the perivascular niche (1), although we did find that the mean number of Sox2$^+$ cells was higher than the mean number of Iba1$^+$ cells within a 25-μm-radius of the nearest blood vessel (Fig. 1D).

These observations were confirmed using an established immunocompetent mouse model in which GBM tumors were induced by PDGF-B and then treated for 2 weeks with rat anti-mouse-VEGF-A IgG followed by euthanasia. CD44$^+$ marks cancer stem-like cells in this model (32) and we found that they also express Sox2 (Supplementary Fig. S1D). Tumor sections were stained with antibodies to CD44 or Iba1, as well as vWf, and the fluorescent intensity of rat anti-mouse-VEGF-A IgG quantified. We found that both perivascular CD44$^+$ and Iba1$^+$ cells within a 25-μm radius of blood vessels internalized anti-mouse-VEGF-A. The rat anti-mouse-VEGF-A-intensity was nearly five-fold higher in the CD44$^+$ perivascular cells as compared to that in the Iba1$^+$ perivascular cells (Fig. 1E and F). The distance of CD44$^+$ perivascular cells from the nearest blood vessel was slightly less than that for Iba1$^+$ cells (Fig. 1G).

Bevacizumab induces autophagy in perivascular tumor cells in the xenograft model of GBM

We then determined whether there were differences in apoptosis of the perivascular tumor cells in the bevacizumab- and placebo-treated xenograft tumors by double labeling for cleaved caspase-3 and Sox2. We did not find a significant difference in the numbers of apoptotic Sox2$^+$ cells in bevacizumab-treated as compared to placebo-treated tumors ($P = 0.50$; Fig. 2A and B). To determine whether bevacizumab induced autophagy, we examined the colocalization of LC3 puncta with LAMP2 (33). We found a significantly higher number and greater area of LC3 puncta colocalized with LAMP2 in the bevacizumab-treated as compared to the placebo-treated tumors (Fig. 2C–E), suggesting that bevacizumab therapy of GBM xenografts induces autophagy *in vivo*.

Internalization of bevacizumab by CD133$^+$ cells from GBM into actin-containing membrane ruffles that is blocked by an inhibitor of macropinocytosis

To confirm that CD133$^+$ cells are able to take up bevacizumab, we analyzed CD133$^+$ cells isolated from xenograft tumors from two different patients with GBM. The CD133$^+$ cells are also Sox2$^+$ (Supplementary Fig. S1E). The cells were seeded on laminin in NBM without EGF and bFGF to replicate the nutrient-starved condition in GBM tumors. We found that, under these conditions, bevacizumab was internalized rapidly (5 minutes) by the CD133$^+$ cell isolates from both patients (Fig. 3A).

Double-label immunofluorescence of the CD133$^+$ cells for actin (Alexa Fluor 488-phalloidin; green) and bevacizumab (Alexa Fluor 647-anti-human IgG; magenta) showed that bevacizumab was internalized into membrane ruffles surrounded by actin (Fig. 3B). This was suggestive of macropinocytosis, which is differentiated from other types of endocytosis by the requirement for remodeling of the actin cytoskeleton with polymerized actin in membrane ruffles. Macropinocytosis is blocked by inhibitors of the Na(+)/H(+) ion exchange pump, such as 5-(N-ethyl-N-isopropyl)amiloride (EIPA; refs. 16, 18, 34), and tetramethylrhodamine (TMR)-70-kDa-Dextran is known to be internalized by macropinocytosis (18). The macropinocytic capabilities of the CD133$^+$ cells were confirmed by their rapid internalization of TMR-70-kDa-Dextran (5 minutes) through a mechanism that was inhibited by EIPA (Fig. 3C and D). The internalization of bevacizumab by the two isolates of CD133$^+$ cells was inhibited significantly by pretreatment with EIPA (Fig. 3E and F). In contrast, the internalization of bevacizumab was not inhibited

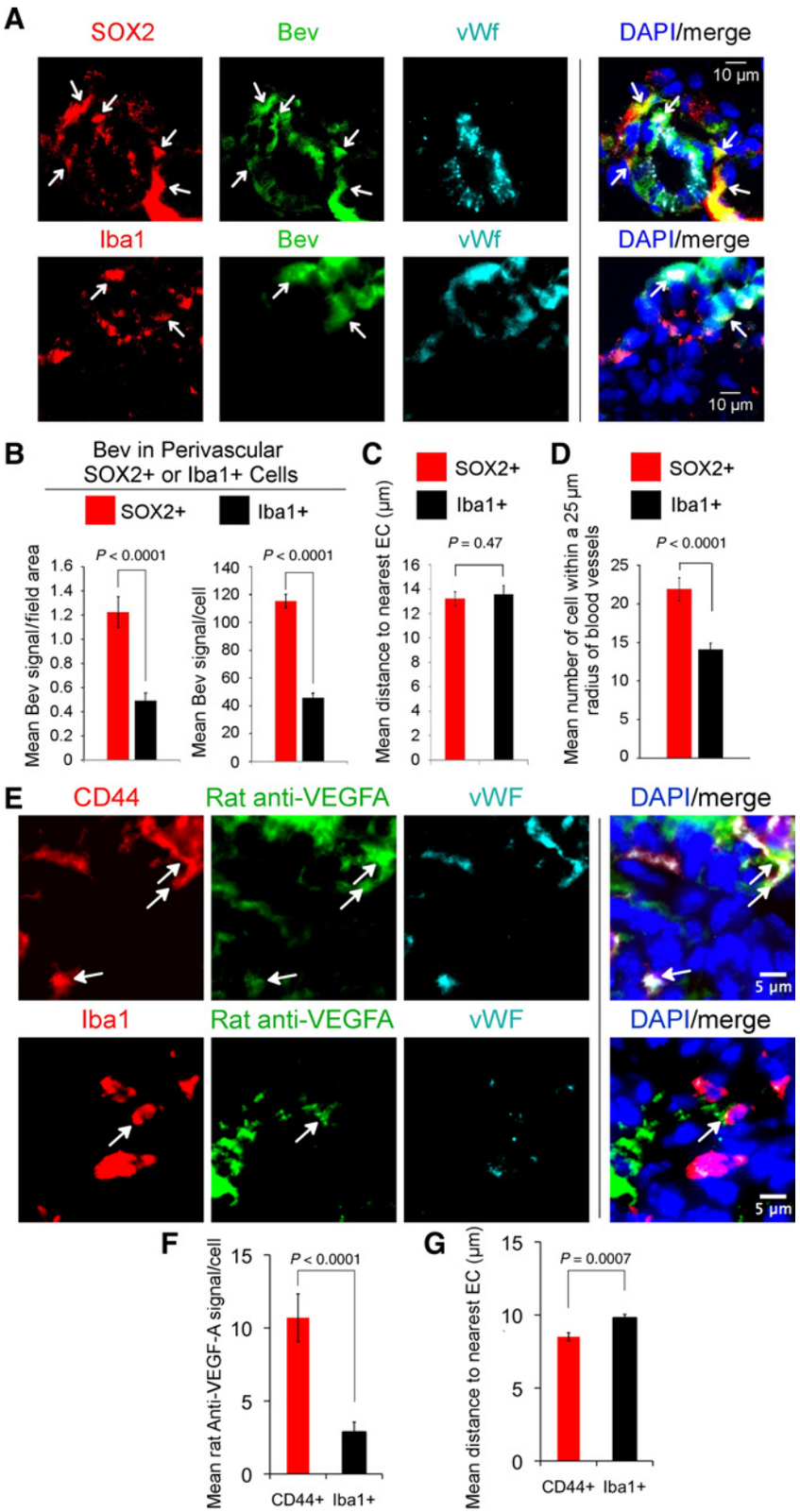

Figure 1.

Bevacizumab gains access to the perivascular tumor space and is internalized predominantly by perivascular Sox2$^+$/CD44$^+$ tumor cells in PDX xenograft and syngeneic mouse models of GBM. **A–D,** PDX GBM tumors (G39 or G59) were injected intracerebrally into the nude mouse (300,000 cells), and treatment with bevacizumab (5 mg/kg, i.p., 2×/week) or placebo initiated on day 13 (G39) or day 28 (G59). Treatment was continued until the development of neurologic signs at day 23 (G39) or day 50 to 77 (G59), followed by euthanasia, brain harvest, freezing in OCT media, and storage at −80°C. Sections from three mouse tumors from each of the two GBM xenografts treated with bevacizumab were reacted with Alexa Fluor 488-anti-hIgG (green) and anti-Sox2 (2.5 μg/mL) or anti-Iba1 (0.5 μg/mL) antibody (red), and rabbit or mouse anti-vWf (5 or 2 μg/mL, respectively) antibody (blue), followed by Alexa Fluor 594-conjugated- and Alexa Fluor 647-conjugated secondary antibodies and DAPI nuclear stain (**A**). Area of tumor from mouse administered bevacizumab shown. Arrows denote bevacizumab in Sox2$^+$ tumor cells or in Iba1$^+$ activated microglia/macrophages (**A**). Scale bars denote 10-μm (**A**). Bevacizumab fluorescent intensity in Sox2$^+$ or in Iba1$^+$ perivascular cells was quantitated as the mean signal intensity/field area and as the mean signal/cell using ImageJ in the six bevacizumab-treated G39 and G59 GBM xenograft tumors (**B**). The mean distance of bevacizumab-positive Sox2$^+$ or Iba1$^+$ perivascular cell from the nearest EC was quantitated using ImageJ on the same six xenograft tumors (**C**). The mean number of Sox2$^+$ or Iba1$^+$ cells within a 25-μm radius of vWf-positive blood vessels was quantitated on the same six xenograft tumors (**D**). **E–G,** The syngeneic somatic gene transfer model of GBM was generated by intracerebral injection of four 6- to -8-week-old *Ntv-a/ink4a-arf*$^{-/-}$ mice with RCAS-PDGF-B-HA. After 4 weeks, treatment with rat anti-mouse VEGF-A IgG (5 mg/kg, i.p., 2×/week) was initiated and continued for 2 weeks, followed by euthanasia, brain harvest, fixation in 4% paraformaldehyde, immersion in sucrose and freezing (−80°C). Tumor bearing sections (5-μm) were reacted with Alexa Fluor 488-anti-rat IgG (green), sheep anti-mouse CD44 (5 μg/mL), or rabbit anti-Iba1 (red), and rabbit or mouse anti-vWf, respectively (as above) (blue), followed by Alexa Fluor 594 and Alexa Fluor 647-conjugated secondary antibodies, and DAPI nuclear stain (**E**). Rat anti-mouse-VEGF-A fluorescent intensity in CD44$^+$ or in Iba1$^+$ perivascular cells was quantitated as the mean signal intensity/cell using ImageJ in the four mice (**F**). The mean distance of rat anti-mouse-VEGF-A-positive CD44$^+$ or Iba1$^+$ perivascular cell from the nearest EC was quantitated using ImageJ on the same four tumors (**G**). Statistical analyses in panels **B–D**, **F** and **G**: linear mixed model.

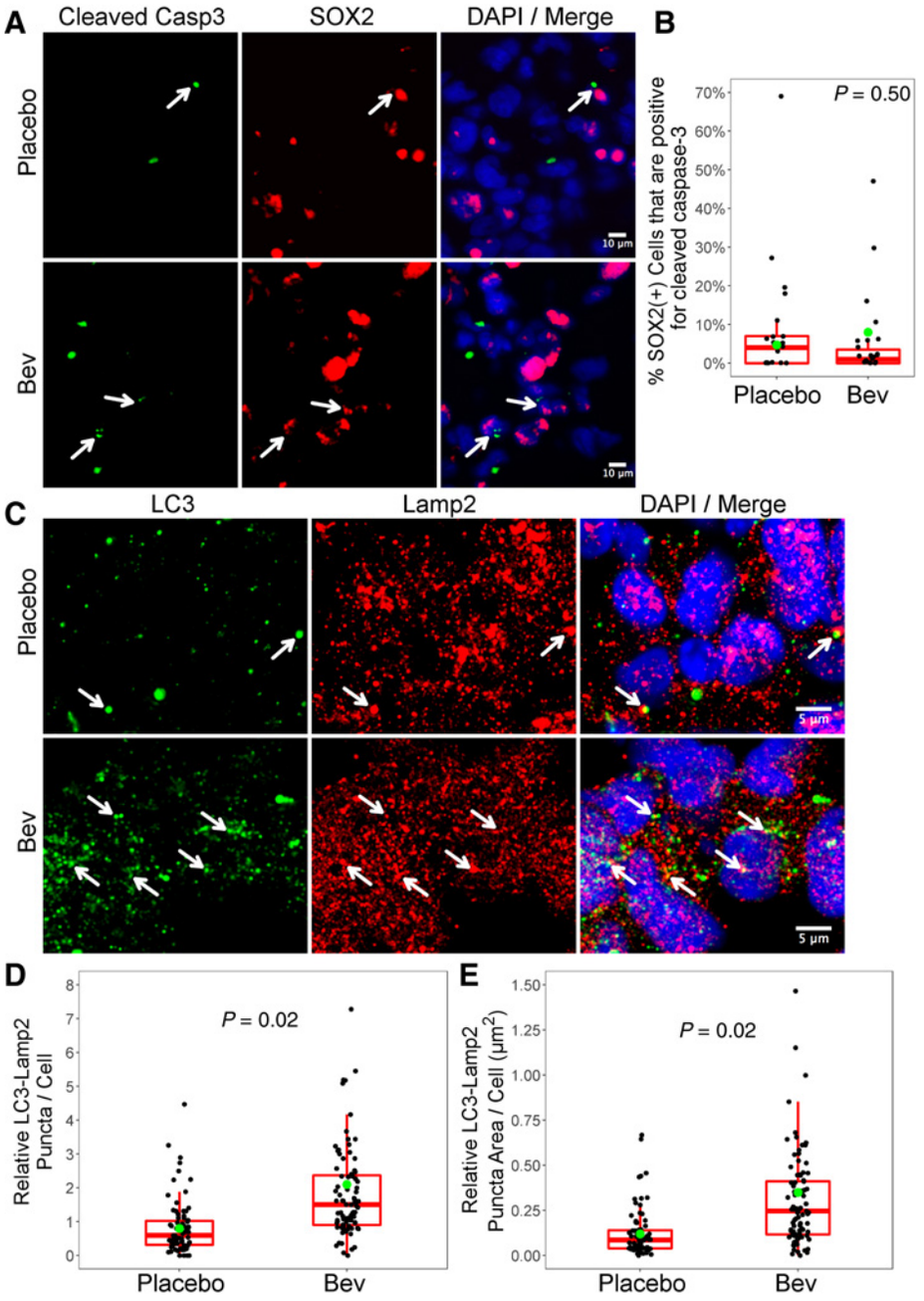

Figure 2.

Bevacizumab treatment of an orthotopic xenograft model of GBM induces autophagy. **A** and **B,** Sections of xenograft GBM tumor from the G39 and G59 PDX tumors treated with bevacizumab or placebo were reacted with rabbit anti-cleaved caspase-3 (0.2 μg/mL; green) and mAb anti-Sox2 (2.5 μg/mL; red) antibodies, followed by Alexa Fluor 488 and Alexa Fluor 594-conjugated secondary antibodies, DAPI nuclear stain and confocal microscopy. Representative photographs of tumor are shown (**A**). Quantitation of the number of double-labeled cleaved caspase-3 and $Sox2^+$ cells in five representative fields/tumor (**B**). Data are graphed as Box and Whisker plots. **C–E,** Sections of xenograft GBM tumor from the G39, G59, and G44 PDX tumors treated with bevacizumab or placebo were reacted with anti-LC3 (2 μg/mL) and anti-LAMP2 (4 μg/mL) antibodies, followed by Alexa Fluor 488 and Alexa Fluor 594-conjugated secondary antibodies, DAPI nuclear stain and confocal microscopy. Representative photographs of tumor are shown (**C**). Quantitation of the number of LC3-LAMP2-positive puncta/cell in 10 representative fields/tumor (**D**); the adjusted means are 2.1 vs. 0.8 for bevacizumab-treated vs. placebo-treated tumors, respectively ($P = 0.02$). Quantitation of the area of LC3-LAMP2-positive puncta/cell in 10 representative fields/tumor (**E**); the adjusted means are 0.35 vs. 0.12 for bevacizumab-treated vs. placebo-treated tumors, respectively ($P = 0.02$). Data are graphed as Box and Whisker plots; the green dots represent the adjusted means. In **D**, two data points in the bevacizumab-treated group (10.36 and 14.73) were removed for graphing purposes, but were included in the statistical analysis. In **E**, one data point in the bevacizumab-treated group (3.23) was removed for graphing purposes, but was included in the statistical analysis. Statistical analyses **B**, **D,** and **E**: linear mixed model.

significantly by EIPA pretreatment of the paired nonstem tumor cells (Fig. 3G and Supplementary Fig. S2). Taken together, these data suggest that $CD133^+$ cells, but not the paired $CD133^-$ (nonstem) tumor cells, utilize macropinocytosis to internalize bevacizumab.

In $CD133^+$ cells from GBM, a fraction of bevacizumab colocalizes with a marker of a recycling compartment and a fraction with a marker of the late endosome/lysosome

Internalized receptors or proteins can be recycled to the cell surface or targeted for degradation. The routes are differentiated based on their kinetics and the markers expressed on the intracellular vesicles. Rab4 marks a "fast" recycling compartment ($t_{1/2}$ ~5 minutes) and also is involved in "slower" recycling through the endosomal recycling complex ($t_{1/2}$ ~15–30 minutes; refs. 17, 35). LAMP1 is a marker of the late endosome/lysosome (17). We therefore examined the colocalization of bevacizumab with Rab4 and LAMP1 (17, 35). $CD133^+$ cells were seeded as described above on laminin and colocalization determined at various time points after treatment with bevacizumab. Rapid, transient colocalization with Rab4 was observed. At 5 minutes bevacizumab was predominantly (68%) colocalized with Rab4, with this colocalization dissipating at 30 min (20%; Fig. 4A and B). At 3 hours, a large fraction of bevacizumab was colocalized with LAMP1

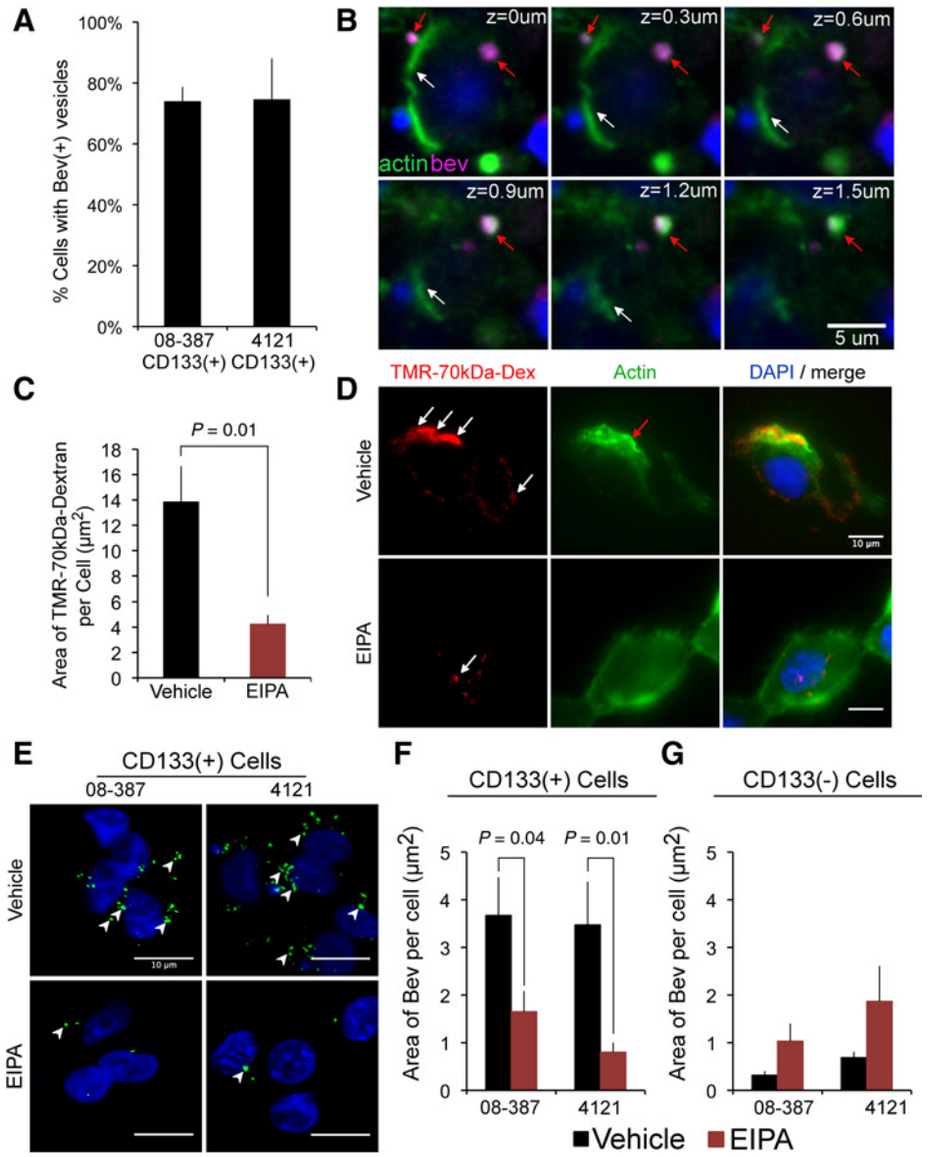

Figure 3.

Bevacizumab is internalized by CD133$^+$ cells into membrane ruffles in a mechanism consistent with macropinocytosis. **A** and **B,** CD133$^+$ cells were plated onto laminin in NBM without bFGF or EGF for 18 hours (37°C, 5% CO_2), followed by the addition of bevacizumab (250 µg/mL) for 5 minutes, the cells washed, fixed, reacted with Alexa Fluor 647-anti-human IgG (5 µg/mL) and Alexa Fluor 488-phalloidin (5 units/ml), followed by DAPI nuclear stain, cover slipping, and confocal microscopy. Percent of CD133$^+$ cells from two different tumor isolates (08-387 and 4121) containing bevacizumab-positive vesicles (**A**). A z-stack of the double-labeling is shown (CD133$^+$ 08-387 cells; **B**). White arrows denote phalloidin-stained cell membrane (green), and red arrows denote bevacizumab-positive vesicle (magenta) surrounded by actin. Scale bar denotes 5-µm. **C** and **D,** CD133$^+$ cells (08-387) treated with 50 µmol/L EIPA or vehicle for 30 minutes (37°C, 5% CO_2), followed by addition of TMR-70-kDa-Dextran (1 mg/mL; red) for 5 minutes, were washed, reacted with Alexa Fluor 488-Phalloidin (green), nuclei stained with DAPI, cover slipped, and microscopy performed. In cells treated with vehicle, TMR-70-kDa-Dextran is found in membrane ruffles (white arrows), containing polymerized actin (red arrows; **D**). In cells treated with EIPA, reduced amounts of TMR-70-kDa-Dextran are internalized (**C** and **D**). The area (µm^2) of TMR-70-kDa-Dextran/cell is plotted as the mean ± SEM from >100 cells/condition (**C**). **E–G,** CD133$^+$ GBM cells (08-387 and 4121) were plated on laminin in NBM as in **A–D**, and paired nonstem tumor cells (CD133$^-$ 08-387 and 4121) were plated in DMEM with 10% FBS for 18 hours. CD133$^+$ cells or the paired CD133$^-$ tumor cells were treated with vehicle or 50 µmol/L EIPA for 30 minutes as above, followed by addition of bevacizumab (5 minutes), and the cells washed, fixed, reacted with Alexa Fluor 488-anti-human IgG, followed by DAPI nuclear stain, cover slipping and microscopy. Arrowheads denote bevacizumab-positive vesicles which are reduced in CD133$^+$ cells treated with EIPA (**E** and **F**) but are not reduced in CD133$^-$ tumor cells treated with EIPA (**G**). The area (µm^2) of bevacizumab/cell is plotted as the mean ± SEM from >100 cells/condition (**F** and **G**). Scale bars denote 10-µm. Statistical analyses: exact two-sided Wilcoxon rank-sum tests.

(~55%; Fig. 4C and D). Similar results were observed on analysis of CD133$^+$ cells isolated from a different GBM tumor (Supplementary Fig. S3A and S3B). Analysis of hIgG by CD133$^+$ cells using the same protocol revealed a similar pattern of trafficking (Supplementary Fig. S3C and S3D). In sections from three different tumor-bearing mice administered bevacizumab, we found

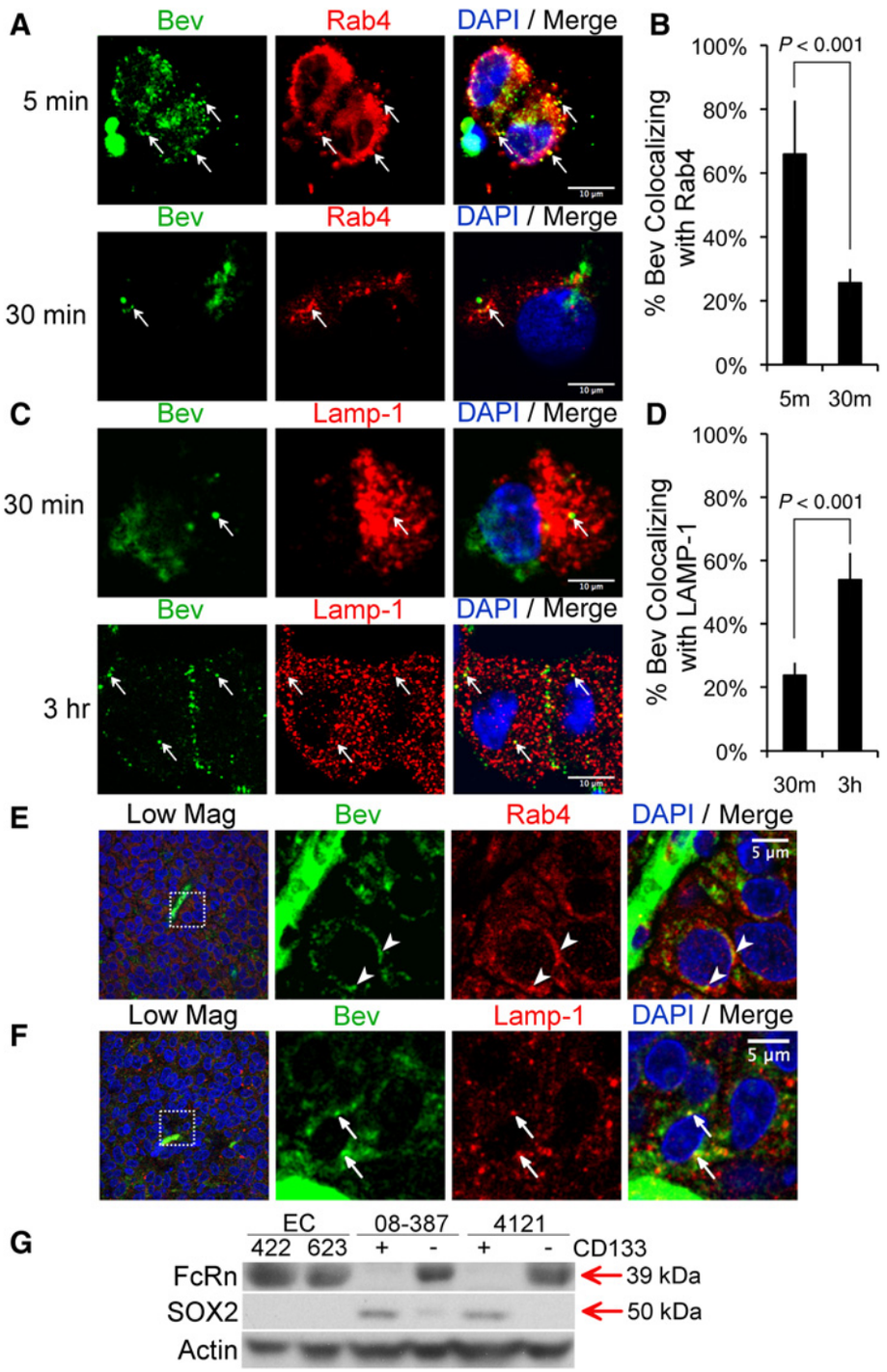

Figure 4.

Colocalization of a fraction of bevacizumab with Rab4 and a fraction with LAMP1 in CD133$^+$ cells *in vitro* and in Sox2$^+$ perivascular tumor cells *in vivo*. **A–D,** CD133$^+$ GBM cells (08-387) were plated for 18 hours as in Fig. 3, followed by addition of bevacizumab (250 μg/mL) for 5 minutes, the cells washed and fixed or the media replaced and the cells washed and fixed at the indicated times. The cells were reacted with Alexa Fluor 488-anti-human IgG and anti-Rab4 (1:33 dilution of lot #OL196003) or anti-LAMP1 (3.3 μg/mL) antibody, Alexa Fluor 594-conjugated secondary antibody, and DAPI nuclear stain, followed by confocal microscopy. Arrows denote colocalization of bevacizumab (green) with Rab4 or LAMP1 (red) (**A** and **C**). The percent bevacizumab colocalized with Rab4 or LAMP1 is plotted as the mean ± SEM at the indicated times based on the Mander's coefficient (**B** and **D**). Statistical analyses: **B** and **D**, Two-sided exact Wilcoxon rank-sum tests. Scale bars denote 10 μm. **E** and **F,** Sections of xenograft GBM tumor from mice that were treated with bevacizumab as in Supplementary Fig. S1A and S1B were reacted with Alexa Fluor 488-anti-human IgG and anti-Rab4 or anti-LAMP1 antibody, and Alexa Fluor 594-conjugated-secondary antibody, followed by DAPI nuclear stain and confocal microscopy. Arrowheads or arrows denote colocalization of bevacizumab (green) with Rab4 (red; **E**) or with LAMP1 (red; **F**). The box in the far-left image in **E** and **F** is magnified in the subsequent images. Scale bar denotes 5 μm. **G,** CD133$^+$ cells (08-387 and 4121) were detergent lysed from cells in suspension culture in NBM without addition of EGF and bFGF; CD133$^-$ nonstem tumor cells cultured in DMEM with 10% FBS were washed and lysed; and primary brain ECs (isolate nos. 422 or 623) plated on collagen in the recommended media with 10% FBS were washed and detergent lysed. Lysates (50 μg per sample) were electrophoresed on SDS-PAGE, and Western blotted with the indicated antibodies.

colocalization of bevacizumab with Rab4 or LAMP1 in perivascular tumor cells (Fig. 4E and F), suggesting similar trafficking of bevacizumab in a xenograft mouse model of GBM as found in CD133$^+$ cells *in vitro*. Similar trafficking of rat IgG was found in perivascular tumor cells in the established immunocompetent model of GBM treated with rat anti-mouse-VEGF-A (Supplementary Fig. S3E and S3F).

FcRn is known to recycle human IgG in ECs (13, 14). We confirmed that FcRn expression was detectable in isolates of normal brain ECs (376 and 422) by Western blotting using two different FcRn-specific antibodies. However, FcRn expression was not detectable in CD133$^+$ cell isolates on Western blotting using either of these antibodies (Fig. 4G and Supplementary Fig. S3G and S3H). FcRn was detectable in the isolates of the paired

$CD133^-$ nonstem tumor cells (Fig. 4G). On stripping of the membrane and reprobing for Sox2, Sox2 expression was detected in the $CD133^+$ cells, whereas a faint band representing Sox2 was detectable in one isolate of the $CD133^-$ nonstem tumor cells (Fig. 4G). Sections from five xenograft tumors were double-labeled for FcRn and vWf, or FcRn and Sox2, and we found 72% of the FcRn fluorescence (adjusted mean) colocalized with vWf in endothelial cells and 16% of the FcRn fluorescence (adjusted mean) colocalized with $Sox2^+$ cells (Supplementary Fig. S4), suggesting that the large majority of $Sox2^+$ cells do not express FcRn *in vivo*. As it has been suggested that FcγRIIB can recycle immune complexes in dendritic cells (36), we also examined expression of FcγRIIB on the $CD133^+$ cells. Myeloma cells (MM.1R) transduced with FcγRIIB were used as a positive control. FcγRIIB was not detected on the $CD133^+$ cells (Supplementary Fig. S3G and S3H).

Bevacizumab binds VEGF-A with high affinity and $CD133^+$ cells from GBM synthesize and secrete VEGF-A. Potentially, the bevacizumab-VEGF-A complex could be trafficked differently from free bevacizumab. To characterize the trafficking of bevacizumab-VEGF complexes in $CD133^+$ cells, biotinylated-VEGF-A was incubated with bevacizumab for 1 hour and the mixture added to the $CD133^+$ cells for 5 minutes, and either fixed or fresh media added for 3 hours before fixing. In this experiment, the Mander's coefficient was calculated as a measure of the percentage of bevacizumab (green) colocalized with VEGF (magenta) that was colocalized with Rab4 or LAMP1 (red; ImageJ with JACoP-plug-In). At 5 minutes, 76% of the bevacizumab-VEGF complex was colocalized with Rab4 (Supplementary Fig. S5A and S5C), and at 3 hours, 47% was colocalized with LAMP1 (Supplementary Fig. S5B and S5D). These data suggest that in the GBM $CD133^+$ cells, the unbound bevacizumab and the bevacizumab–VEGF-A complex are trafficked similarly.

Effects of bevacizumab on the expression of VEGF-A&C and PGF by $CD133^+$ cells

Bevacizumab neutralizes VEGF-A and, thus, could induce VEGF-A-depletion in treated cells. VEGF-C also binds VEGFR2 and activates its signaling (37). Bevacizumab can induce expression of PGF (a VEGF family member), which binds and activates VEGFR1 and may indirectly activate VEGFR2 through several mechanisms (38, 39). Therefore, we examined the expression of VEGF-A&C and PGF in the $CD133^+$ cells plated as above (in the absence of added growth factors) and treated with bevacizumab. VEGF-A, VEGF-C, and PGF were detected in the media of $CD133^+$ cells, and the levels increased from 24 to 48 hours (Fig. 5A–C). With bevacizumab treatment, the levels of VEGF-A were markedly reduced whereas the levels of VEGF-C and PGF were unchanged (Fig. 5A–C). Although there was a reduction in phospho-VEGFR2 in the $CD133^+$ cells on bevacizumab depletion of VEGF-A, phospho-VEGFR2 was still detectable (Supplementary Fig. S6A and S6B).

Macropinocytosis of bevacizumab promotes proliferation of $CD133^+$ cells and bevacizumab depletion of VEGF-A induces a prosurvival autophagy

To determine whether bevacizumab depletion of VEGF-A induced autophagy in the $CD133^+$ cells, we examined the colocalization of LC3 puncta with the lysosomal marker LAMP2 (33), as well as examining the effect of bevacizumab on cell cytotoxicity/death and viability/proliferation. The concentration of bevacizumab we used had been reported previously to induce autophagy in GBM and cancer stem cell-like GBM cells (40). We found significantly higher autophagy and no change in cell death in bevacizumab-treated $CD133^+$ cells as compared to vehicle at 24 hours (Fig. 5D and E). Treatment with hIgG at the same concentration decreased autophagy and had no effect on cell death at 24 hours (Fig. 5D and E). Downregulation of VEGF-A with siRNA in the $CD133^+$ cells increased the colocalization of LC3 puncta with LAMP2 as compared to the control siRNA at 48 hours (Supplementary Fig. S6C), suggesting bevacizumab depletion of VEGF-A in the media causes a growth factor-starvation-induced autophagy. To optimally assess viability/proliferation, an MTT assay was performed at 48 hours, and indicated that bevacizumab treatment resulted in higher viability/proliferation as compared to the vehicle control (Fig. 5F). These results suggest macropinocytosis of IgG, followed by its lysosomal trafficking and nonspecific degradation provided basic building blocks that promoted viability/proliferation. Blocking macropinocytosis of bevacizumab with EIPA treatment at 48 hours significantly increased autophagy and cell death (Fig. 5G and H). EIPA treatment also increased autophagy and cell death in vehicle-treated $CD133^+$ cells, but the increase in cell death was greater in the absence of bevacizumab treatment (Fig. 5G). Treatment with BafilomycinA1, which blocks lysosomal acidification and autophagy (33), caused a significant reduction in colocalization of LC3 puncta with LAMP2 in the bevacizumab-treated $CD133^+$ cells and an increase in cell death (Fig. 5G and H). Taken together, these data suggest that macropinocytosis and lysosomal trafficking of bevacizumab and other proteins promotes $CD133^+$ cell survival and proliferation *in vitro*, and that autophagy induced by bevacizumab depletion of VEGF-A also promotes survival.

Trafficking of bevacizumab in GBM does not involve significant transcytosis across normal brain ECs or ECs isolated from GBM tumors (TECs)

Transcytosis (reviewed in ref. 41) across ECs is regulated in normal brain, but potentially could be abnormal in TECs. Using a standard *in vitro* transcytosis assay for normal brain ECs (41), we compared transcytosis of bevacizumab across monolayers of normal brain ECs and TECs. Quantitation of bevacizumab in the lower chamber by ELISA assay showed that ∼30% of bevacizumab was transcytosed across both normal brain ECs and TECs over 2 hours (Supplementary Fig. S7A). There was a two-fold larger permeability coefficient for 70-kDa-FITC-Dextran in TECs as compared to the normal brain ECs (Supplementary Fig. S7B). Both normal brain ECs and TECs internalized bevacizumab over 30 minutes (Supplementary Fig. S7C and S7D). Collectively, these data suggest that transcytosis of bevacizumab is not enhanced in TECs, supporting the concept that bevacizumab gains access to the perivascular tumor space in GBM due to alterations in the BBB.

Discussion

We demonstrate that bevacizumab gains access to the perivascular tumor niche in established orthotopic mouse models of GBM through the well-described alterations in the BBB, suggesting that vascular normalization by bevacizumab does not occur in 100% of tumor vessels. We found that the $CD133^+/Sox2^+$ cells and the paired nonstem tumor cells can internalize bevacizumab but do so through different mechanisms and that, *in vivo*, $Sox2^+/$

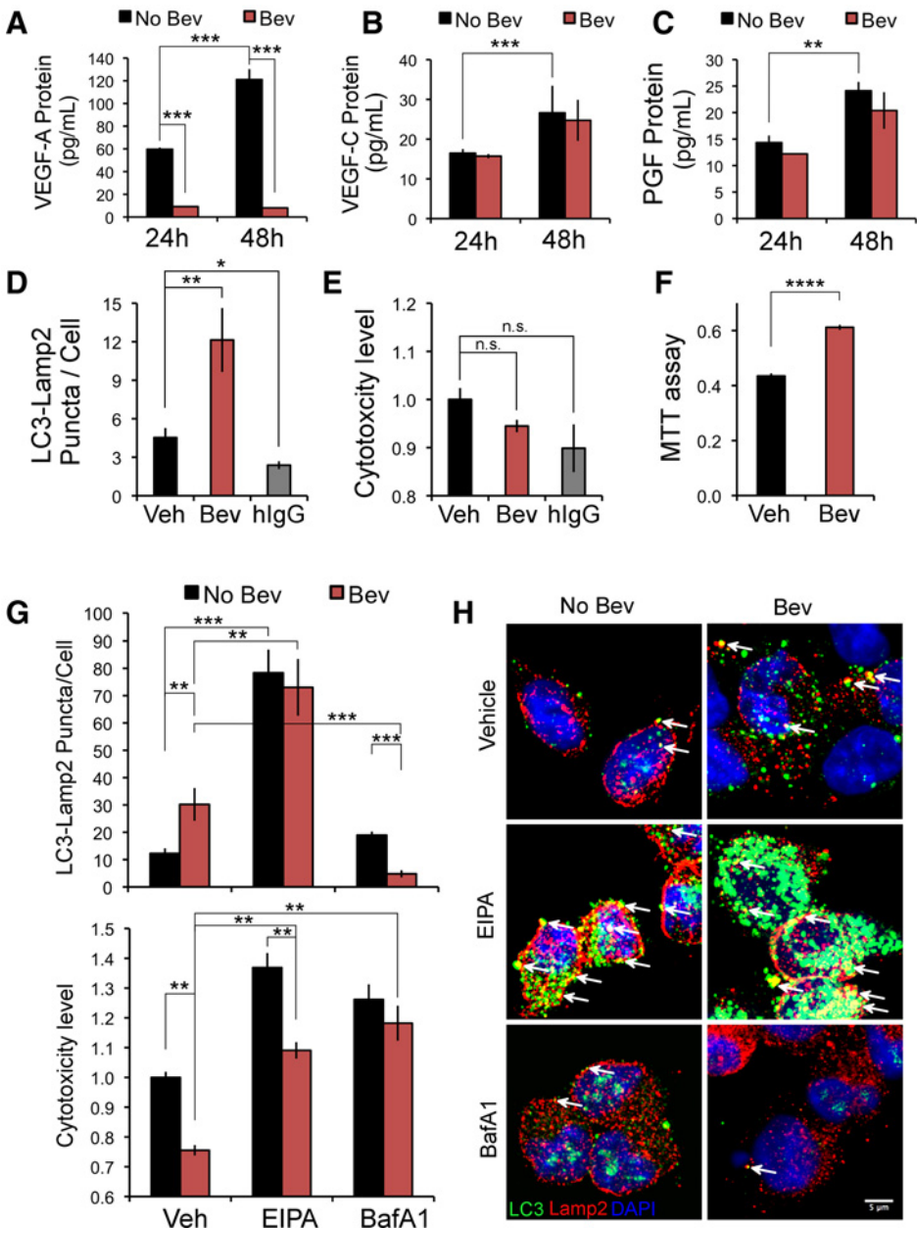

Figure 5.

Bevacizumab trafficking in CD133$^+$ cells affects two survival pathways. CD133$^+$ cells were plated as in Fig. 3 in NBM without addition of EGF and bFGF, treated with bevacizumab or hIgG for 24 or 48 hours (1 mg/mL), and the media removed for ELISA assay (**A–C**), or the cells washed, fixed and reacted with anti-LC3 antibody (2 μg/mL; green) and anti-LAMP2 antibody (4 μg/mL; red), followed by Alexa Fluor 488 and Alexa Fluor 594-conjugated secondary antibodies, DAPI nuclear stain and confocal microscopy (**D**, **G,** and **H**), or the cells subjected to a cytotoxicity/death assay (**E** and **G**) or an MTT assay (**F**). **A–C,** Levels of VEGF-A or VEGF-C or PGF protein in the media of CD133$^+$ cells treated with bevacizumab or vehicle are graphed as the mean ± SEM at the time points shown. The levels of VEGF-A with bevacizumab treatment at 24 and 48 hours were 9.18 ± 0.32 and 8.04 ± 0.34 pg/mL (mean ± SEM), respectively. **D,** Colocalization of LC3-LAMP2 puncta/cell in CD133$^+$ cells treated with bevacizumab, hIgG or vehicle for 24 hours. Quantitation of the area of colocalization (ImageJ) from 10 fields/condition is graphed as the mean ± SEM. **E,** Quantitation of cell cytotoxicity/death (relative to vehicle) after bevacizumab, hIgG or vehicle treatment for 24 hours, and graphed as the mean ± SEM. **F,** Quantitation of viability/proliferation in CD133$^+$ cells treated with bevacizumab or vehicle for 48 hours. **G** and **H,** Colocalization (ImageJ) of LC3 puncta with LAMP2 (10 fields/condition) or quantitation of cell cytotoxicity/death (relative to vehicle) is shown in CD133$^+$ cells treated with bevacizumab or vehicle for 48 hours, with or without inhibitors, and is graphed as the mean + SEM (**G**). Representative images of the colocalization of the LC3-LAMP2 puncta in the same six conditions is shown (**H**). Arrows denote colocalization (yellow) (**H**). Statistical analyses: **A–C** and **F**, two-sided exact Wilcoxon rank-sum tests; **D** and **E**, the Steel Method; and **G**, Wilcoxon rank-sum tests. *, $P < 0.05$; **, $P < 0.01$; ***, $P < 0.001$; and ****, $P < 0.0001$. n.s., denotes not significant.

$CD44^+$ perivascular tumor cells appear to largely be responsible for anti-VEGF-A IgG internalization. We further show that the intracellular trafficking of anti-VEGF-A IgG in GBM tumors affects the survival of $CD133^+/Sox2^+$ cells.

Under the conditions used in these experiments, the $CD133^+$ cells internalized bevacizumab and hIgG through the process of macropinocytosis, based on our observation of actin-enriched plasma membrane ruffles surrounding and engulfing bevacizumab into large vesicles and significant inhibition of internalization by EIPA. Although macropinocytosis appeared to be the primary mechanism underlying the internalization of bevacizumab in the $CD133^+$ cells, we cannot rule out the possibility of a minor role for another clathrin-independent mechanism. The paired nonstem tumor cells internalized much less bevacizumab and, as the internalization was not affected significantly by treatment with EIPA, macropinocytosis did not appear to contribute to the internalization in these cells.

Analysis of the intracellular trafficking of bevacizumab and hIgG *in vitro* showed colocalization with established markers of endocytic compartments in $CD133^+$ cells, providing clues to the potential fate of the internalized bevacizumab. Under the experimental conditions without added growth factors, bevacizumab was largely colocalized with a marker of a "fast" recycling compartment (Rab4) at 5 minutes. This would suggest that a considerable amount of the internalized bevacizumab is recycled rapidly to the extracellular environment where it would be available to bind and neutralize VEGF-A. FcRn has been shown to be responsible for the recycling of endogenous IgG in ECs and several other cell types (reviewed in ref. 13). The time course for bevacizumab and human IgG recycling by the $CD133^+$ cells was faster than has been described for FcRn (14). Moreover, we found that the $CD133^+/Sox2^+$ cells do not express FcRn by Western blot analysis and that the large majority of $Sox2^+$ perivascular tumor cells do not express FcRn *in vivo*. Thus, FcRn was unlikely to play a role in the recycling of bevacizumab and hIgG in the $CD133^+$ cells. Similarly, the inhibitory FcγRIIB has been shown to endocytose and recycle immune complexes back to the cell surface on dendritic cells (36), but we did not detect FcγRIIB on the $CD133^+$ cells by Western blotting. The isoelectric point (p*I*) of humanized IgG mAbs has been shown to affect clearance with a higher p*I* promoting clearance in a manner that was FcRn independent and presumed to be due to an increased rate of fluid phase endocytosis (reviewed in ref. 42). Bevacizumab has a higher p*I* ($pI = 8.3$; http://www.drugbank.ca) than endogenous IgG ($pI = 7.2$). Although we did not compare the rates of internalization of bevacizumab and hIgG, we did find similar trafficking patterns in the $CD133^+$ cells.

Delivery of the endosome cargo to the late endosome/lysosome is slower than its delivery to the recycling compartment (17). We found that in the $CD133^+$ cells a large amount of bevacizumab colocalized with a marker of the late endosome/lysosome (LAMP1) at 3 hours. This is consistent with the report of localization of bevacizumab to the lysosome in retinal ECs at 72 hours posttreatment *in vitro* (43). This localization to the lysosome suggests that the $CD133^+$ cells in the perivascular tumor space also degrade bevacizumab. The percentage of bevacizumab localized to the LAMP1 compartment is probably an underestimate as that pool of bevacizumab is undergoing degradation. In the early endosome, differential sorting of cargo protein to a recycling compartment or the lysosome can be based on specific cargo protein signals (17), including ubiquitination that signals sorting of membrane proteins to the lysosome (44).

The trafficking of the bevacizumab–VEGF-A complex was similar to the trafficking of bevacizumab alone in the $CD133^+$ cells; a fraction colocalized with a marker of the "fast" recycling compartment (Rab4) at 5 minutes (75%) and a fraction colocalized with a marker of the late endosome/lysosome (LAMP1; 47%) at 3 hours. In ECs, the VEGF–VEGFR2 complex is known to be internalized and recycled by different mechanisms, including clathrin-coated pit and endophilin-dependent mechanisms (45, 46), but in tumor cells the internalization and trafficking of the VEGF–VEGFR2 complex is not as well-defined.

We show that bevacizumab trafficking directly affects two survival pathways in the $CD133^+$ cells. First, bevacizumab in the perivascular space depletes $CD133^+$ cell-secreted VEGF-A causing a growth factor-deprivation-induced autophagy. This is demonstrated by the significantly higher number and area of LC3-LAMP2 puncta when the $CD133^+$ cells are treated with bevacizumab as compared to vehicle; an increase in numbers of LC3-LAMP2 puncta when VEGF-A is downregulated with siRNA but not when the cells are treated with control siRNA; and a decrease in LC3-LAMP2 puncta on treatment of the cells with hIgG. BafilomycinA1 treatment (inhibits lysosomal acidification) blocked the increase in number and area of LC3-LAMP2 puncta in $CD133^+$ cells treated with bevacizumab. The significant decrease in cell death with bevacizumab treatment at 48 hours supports the concept that bevacizumab induces a prosurvival form of autophagy in the $CD133^+$ cells. Autophagy is generally a survival mechanism by which cells that are stressed due to nutrient deprivation, absence of growth factors, or hypoxia metabolize organelles, misfolded proteins and aggregated proteins, thereby generating molecules that allow the cell to survive (33, 47). Previously, others have reported an increase in autophagy on bevacizumab treatment of GBM cells cultured in media with growth factors or under hypoxic conditions (40, 48), but the effect of bevacizumab on VEGF-A secreted by tumor cells was not examined. Second, our data suggest that the macropinocytosis of bevacizumab followed by its targeting to the lysosome promotes the survival of $CD133^+$ cells due to the increased availability of basic building blocks (amino acids) for the cell. This is supported by the increased viability/proliferation we observed with bevacizumab treatment, and the significant increase in cell death we observed on inhibition of macropinocytosis using the inhibitor EIPA. EIPA treatment also significantly increased autophagy presumably by blocking the macropinocytosis of nutrients and bevacizumab by the cell. The increase in cell death and autophagy taken together point to the possibility that EIPA induces autophagic cell death. The increase in cell death associated with EIPA treatment was significantly lower in bevacizumab-treated $CD133^+$ cells than vehicle-treated $CD133^+$ cells, and this is likely due to the protective growth factor-deprivation-induced autophagy that bevacizumab promotes in the $CD133^+$ cells.

Macropinocytosis is highly regulated and thought to be stimulated by growth factors (16, 17). The macropinocytosis of bevacizumab by $CD133^+$ cells occurred in the absence of exogenous growth factors, suggesting that an autocrine or paracrine growth factor pathway may be promoting this process, such as the VEGF/VEGFR2 pathway or another growth factor signaling pathway. VEGF-A has been reported to be a pro-angiogenic growth factor secreted by $CD133^+$ cells from GBM (7). Our data support

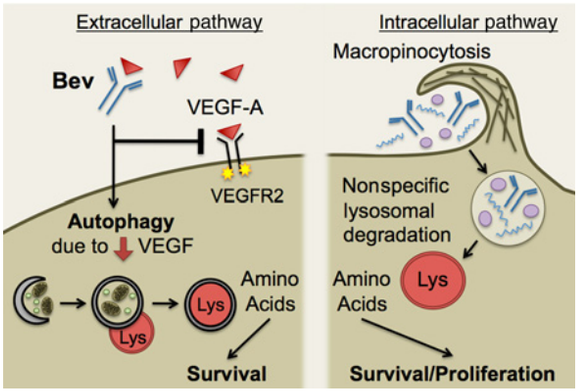

Figure 6.

Schematic depicting the effect of bevacizumab trafficking on two survival pathways in CD133$^+$ cells from GBM. Bevacizumab gains access to the perivascular tumor tissue by leakage across an altered BBB, followed by macropinocytosis by CD133$^+$ cells and trafficking to a Rab4 recycling compartment (not shown) or a LAMP1 lysosomal compartment, as well as bevacizumab neutralization of VEGF-A in the perivascular space inducing autophagy. Macropinocytosis of bevacizumab results in partial trafficking to the lysosome where nonspecific degradation occurs, and this generates amino acids (basic building blocks) for the cell that promotes survival/proliferation. The depletion of VEGF in the extracellular environment by bevacizumab results in growth factor starvation-induced autophagy that also promotes survival.

this concept and further suggest that the CD133$^+$ cells are addicted to VEGF-A. When VEGF-A is depleted by bevacizumab treatment, the cells undergo autophagy. Despite depletion of VEGF-A with bevacizumab, phosphorylated-VEGFR2 was still detectable in CD133$^+$ cells, although the level of phosphorylation was reduced. This could be due to CD133$^+$ cell secretion of VEGF-C, and/or to a ligand-independent VEGFR2 signaling mechanism. Growth factor receptors also can be macropinocytosed by cells, for example, the macropinocytosis and lysosomal targeting of the EGF receptor (EGFR) when bound by a combination of mAb anti-EGFR (cetuximab) and anti-human IgG has been reported in large vessel ECs transfected with EGFR (49).

Our studies of the trafficking of anti-VEGF antibody when administered to established xenograft and syngeneic mouse models of GBM indicate the IgG gains access to the perivascular tumor tissue and is internalized predominantly by perivascular Sox2$^+$/CD44$^+$-tumor cells. Furthermore, in these cells, a fraction of bevacizumab is colocalized with Rab4 and a fraction with LAMP1, suggesting similar trafficking of bevacizumab *in vivo* as we found in CD133$^+$/Sox2$^+$ cells *in vitro*. Supporting our *in vitro* data, in bevacizumab-treated xenograft tumors there was increased colocalization of LC3 puncta with LAMP2 in perivascular tumor cells as compared to placebo-treated tumors, suggesting bevacizumab induced autophagy *in vivo* in the xenograft model. Other investigators have shown that bevacizumab treatment induces autophagy in tumor cells in GBM xenograft models and this was attributed to upregulation of interferon regulatory factor-1 or hypoxia in tumor cells (40, 48).

In summary (Fig. 6), our data suggest that (i) CD133$^+$/Sox2$^+$ cells in media without addition of growth factors macropinocytose bevacizumab, and a fraction is trafficked to a "fast" recycling compartment independent of FcRn and a fraction to the lysosome; (ii) bevacizumab trafficking promotes CD133$^+$ cell survival through two pathways: the macropinocytosis and lysosomal trafficking of bevacizumab that generates basic building blocks for the cell and growth factor deprivation-induced autophagy; and (iii) *in vivo*, anti-VEGF-A antibody localizes to the perivascular tumor tissue suggesting it can target tumor-secreted VEGF, is similarly trafficked in perivascular tumor cells and induces a prosurvival autophagy. It should be noted that we are not suggesting bulk effects on the levels of bevacizumab. Rather, we demonstrate a significant effect on the survival of a population of tumor cells in the perivascular microenvironment that are resistant to radiation and chemotherapy and have been suggested to be cancer stem cell-like cells. We have not addressed whether the uptake of bevacizumab could be affecting other clinically relevant processes, such as the expression of GLUT3 (50), the consequences of the survival of the perivascular cancer stem-like cells after bevacizumab treatment, or the mechanisms that trigger their subsequent expansion and potential aggressive invasiveness (2). As bevacizumab also is used to treat renal, colon, and lung cancer and as we observed similar trafficking of bevacizumab and hIgG, these studies may have applicability to other cancers in which FcRn is not expressed on cancer stem cell-like cells or tumor cells and to other mAb therapeutics.

Disclosure of Potential Conflicts of Interest

M.S. Ahluwalia is a consultant/advisory board member for Abbvie, Astra Zeneca, Bristol-Myers Squibb, CBT Pharmaceuticals, Caris Lifesciences, Incyte, and Monteris Medical, and reports receiving commercial research support from Bristol-Myers Squibb, Novartis and Novocure. No potential conflicts of interest were disclosed by the other authors.

Authors' Contributions

Conception and design: G. Müller-Greven, M.S. Ahluwalia, C.J. Herting, M. Bredel, J.N. Sarkaria, P. Hamerlik, C.L. Gladson
Development of methodology: G. Müller-Greven, C.R. Carlin, C.L. Gladson
Acquisition of data (provided animals, acquired and managed patients, provided facilities, etc.): G. Müller-Greven, M.E. Burgett, A. Lauko, A.S. Nowacki, M.A. Qadan, S.A. Toms, J.D. Lathia, D. Hambardzumyan, J.N. Sarkaria, P. Hamerlik, C.L. Gladson
Analysis and interpretation of data (e.g., statistical analysis, biostatistics, computational analysis): G. Müller-Greven, M.E. Burgett, A.S. Nowacki, M. Bredel, J.D. Lathia, C.L. Gladson
Writing, review, and/or revision of the manuscript: G. Müller-Greven, C.R. Carlin, M.S. Ahluwalia, A. Lauko, A.S. Nowacki, M. Bredel, S.A. Toms, J.N. Sarkaria, C.L. Gladson
Administrative, technical, or material support (i.e., reporting or organizing data, constructing databases): C.L. Gladson
Study supervision: C.L. Gladson

Acknowledgments

We thank Dr. Judy Drazba (Imaging Core) for assistance, Dr. Fiona Hunter for critically reading the manuscript, and Drs. Qing Yi and Qiang Wang for the gift of MM.1R cells transduced with FcγRIIB.

Grant Support

This research was supported by NIH grants R01CA175120 (to C.L. Gladson), U01 CA160882 (to D. Hambardzumyan), R01CA176830 and Mayo Brain Tumor SPORE P50 CA108961 (to J.N. Sarkaria), and Velosano Foundation funding (to C.L. Gladson). The Leica-SP5-confocal/multi-photon microscope utilized was purchased with partial funding from NIH SIG-grant 1S10RR026820-01.

The costs of publication of this article were defrayed in part by the payment of page charges. This article must therefore be hereby marked *advertisement* in accordance with 18 U.S.C. Section 1734 solely to indicate this fact.

Received January 31, 2017; revised August 7, 2017; accepted September 7, 2017; published OnlineFirst September 14, 2017.

References

1. Gilbertson RJ, Rich JN. Making a tumour's bed: glioblastoma stem cells and the vascular niche. Nat Rev Cancer 2007;7:733–6.
2. Lu-Emerson C, Duda DG, Emblem KE, Taylor JW, Gerstner ER, Loeffler JS, et al. Lessons from anti-vascular endothelial growth factor and anti-vascular endothelial growth factor receptor trials in patients with glioblastoma. J Clin Oncol 2015;33:1197–213.
3. Friedman HS, Prados MD, Wen PY, Mikkelsen T, Schiff D, Abrey LE, et al. Bevacizumab alone and in combination with irinotecan in recurrent glioblastoma. J Clin Oncol 2009;27:4733–40.
4. Vredenburgh JJ, Desjardins A, Herndon JE 2nd, Marcello J, Reardon DA, Quinn JA, et al. Bevacizumab plus irinotecan in recurrent glioblastoma multiforme. J Clin Oncol 2007;25:4722–9.
5. Nowosielski M, Wiestler B, Goebel G, Hutterer M, Schlemmer HP, Stockhammer G, et al. Progression types after antiangiogenic therapy are related to outcome in recurrent glioblastoma. Neurology 2014;82:1684–92.
6. Bao S, Wu Q, McLendon RE, Hao Y, Shi Q, Hjelmeland AB, et al. Glioma stem cells promote radioresistance by preferential activation of the DNA damage response. Nature 2006;444:756–60.
7. Bao S, Wu Q, Sathornsumetee S, Hao Y, Li Z, Hjelmeland AB, et al. Stem cell-like glioma cells promote tumor angiogenesis through vascular endothelial growth factor. Cancer Res 2006;66:7843–8.
8. Hamerlik P, Lathia JD, Rasmussen R, Wu Q, Bartkova J, Lee M, et al. Autocrine VEGF-VEGFR2-Neuropilin-1 signaling promotes glioma stem-like cell viability and tumor growth. J Exp Med 2012;209:507–20.
9. Wolburg H, Noell S, Fallier-Becker P, Mack AF, Wolburg-Buchholz K. The disturbed blood-brain barrier in human glioblastoma. Mol Aspects Med 2012;33:579–89.
10. Nduom EK, Yang C, Merrill MJ, Zhuang Z, Lonser RR. Characterization of the blood-brain barrier of metastatic and primary malignant neoplasms. J Neurosurg 2013;119:427–33.
11. Burkhardt JK, Hofstetter CP, Santillan A, Shin BJ, Foley CP, Ballon DJ, et al. Orthotopic glioblastoma stem-like cell xenograft model in mice to evaluate intra-arterial delivery of bevacizumab: from bedside to bench. J Clin Neurosci 2012;19:1568–72.
12. Koch M, de Jong JS, Glatz J, Symvoulidis P, Lamberts LE, Adams AL, et al. Threshold analysis and biodistribution of fluorescently labeled bevacizumab in human breast cancer. Cancer Res 2017;77:623–31.
13. Roopenian DC, Akilesh S. FcRn: the neonatal Fc receptor comes of age. Nat Rev Immunol 2007;7:715–25.
14. Ward ES, Martinez C, Vaccaro C, Zhou J, Tang Q, Ober RJ. From sorting endosomes to exocytosis: association of Rab4 and Rab11 GTPases with the Fc receptor, FcRn, during recycling. Mol Biol Cell 2005;16:2028–38.
15. Swiercz R, Mo M, Khare P, Schneider Z, Ober RJ, Ward ES. Loss of expression of the recycling receptor, FcRn, promotes tumor cell growth by increasing albumin consumption. Oncotarget 2017;8:3528–41.
16. Lim JP, Gleeson PA. Macropinocytosis: an endocytic pathway for internalising large gulps. Immunol Cell Biol 2011;89:836–43.
17. El-Sayed A, Harashima H. Endocytosis of gene delivery vectors: from clathrin-dependent to lipid raft-mediated endocytosis. Mol Ther 2013;21:1118–30.
18. Commisso C, Davidson SM, Soydaner-Azeloglu RG, Parker SJ, Kamphorst JJ, Hackett S, et al. Macropinocytosis of protein is an amino acid supply route in Ras-transformed cells. Nature 2013;497:633–7.
19. Kamphorst JJ, Nofal M, Commisso C, Hackett SR, Lu W, Grabocka E, et al. Human pancreatic cancer tumors are nutrient poor and tumor cells actively scavenge extracellular protein. Cancer Res 2015;75:544–53.
20. Huang P, Rani MR, Ahluwalia MS, Bae E, Prayson RA, Weil RJ, et al. Endothelial expression of TNF receptor-1 generates a proapoptotic signal inhibited by integrin alpha6beta1 in glioblastoma. Cancer Res 2012;72:1428–37.
21. Eyler CE, Foo WC, LaFiura KM, McLendon RE, Hjelmeland AB, Rich JN. Brain cancer stem cells display preferential sensitivity to Akt inhibition. Stem Cells 2008;26:3027–36.
22. Zheng Y, Yang J, Qian J, Qiu P, Hanabuchi S, Lu Y, et al. PSGL-1/selectin and ICAM-1/CD18 interactions are involved in macrophage-induced drug resistance in myeloma. Leukemia 2013;27:702–10.
23. Carlson BL, Pokorny JL, Schroeder MA, Sarkaria JN. Establishment, maintenance and in vitro and in vivo applications of primary human glioblastoma multiforme (GBM) xenograft models for translational biology studies and drug discovery. Curr Protoc Pharmacol 2011;Chapter 14:Unit 14.16.
24. Hambardzumyan D, Amankulor NM, Helmy KY, Becher OJ, Holland EC. Modeling adult gliomas using RCAS/t-va technology. Transl Oncol 2009;2:89–95.
25. Basu A, Contreras AG, Datta D, Flynn E, Zeng L, Cohen TC, et al. Overexpression of vascular endothelial growth factor and the development of post-transplantation cancer. Cancer Res 2008;68:5689–98.
26. Fael Al-Mayhani TM, Ball SL, Zhao JW, Fawcett J, Ichimura K, Collins PV, et al. An efficient method for derivation and propagation of glioblastoma cell lines that conserves the molecular profile of their original tumours. J Neurosci Methods 2009;176:192–9.
27. Gangemi RM, Griffero F, Marubbi D, Perera M, Capra MC, Malatesta P, et al. SOX2 silencing in glioblastoma tumor-initiating cells causes stop of proliferation and loss of tumorigenicity. Stem Cells 2009;27:40–8.
28. Klettner A, Roider J. Comparison of bevacizumab, ranibizumab, and pegaptanib in vitro: efficiency and possible additional pathways. Invest Ophthalmol Vis Sci 2008;49:4523–7.
29. Ryan S, Verghese S, Cianciola NL, Cotton CU, Carlin CR. Autosomal recessive polycystic kidney disease epithelial cell model reveals multiple basolateral epidermal growth factor receptor sorting pathways. Mol Biol Cell 2010;21:2732–45.
30. Yu YJ, Zhang Y, Kenrick M, Hoyte K, Luk W, Lu Y, et al. Boosting brain uptake of a therapeutic antibody by reducing its affinity for a transcytosis target. Sci Transl Med 2011;3:84ra44.
31. Ahmed Z, Shaw G, Sharma VP, Yang C, McGowan E, Dickson DW. Actin-binding proteins coronin-1a and IBA-1 are effective microglial markers for immunohistochemistry. J Histochem Cytochem 2007;55:687–700.
32. Pietras A, Katz AM, Ekstrom EJ, Wee B, Halliday JJ, Pitter KL, et al. Osteopontin-CD44 signaling in the glioma perivascular niche enhances cancer stem cell phenotypes and promotes aggressive tumor growth. Cell Stem Cell 2014;14:357–69.
33. Galluzzi L, Pietrocola F, Bravo-San Pedro JM, Amaravadi RK, Baehrecke EH, Cecconi F, et al. Autophagy in malignant transformation and cancer progression. EMBO J 2015;34:856–80.
34. Koivusalo M, Welch C, Hayashi H, Scott CC, Kim M, Alexander T, et al. Amiloride inhibits macropinocytosis by lowering submembranous pH and preventing Rac1 and Cdc42 signaling. J Cell Biol 2010;188:547–63.
35. van der Sluijs P, Hull M, Webster P, Male P, Goud B, Mellman I. The small GTP-binding protein rab4 controls an early sorting event on the endocytic pathway. Cell 1992;70:729–40.
36. Bergtold A, Desai DD, Gavhane A, Clynes R. Cell surface recycling of internalized antigen permits dendritic cell priming of B cells. Immunity 2005;23:503–14.
37. Joukov V, Pajusola K, Kaipainen A, Chilov D, Lahtinen I, Kukk E, et al. A novel vascular endothelial growth factor, VEGF-C, is a ligand for the Flt4 (VEGFR-3) and KDR (VEGFR-2) receptor tyrosine kinases. EMBO J 1996;15:290–98.
38. Simon T, Coquerel B, Petit A, Kassim Y, Demange E, Le Cerf D, et al. Direct effect of bevacizumab on glioblastoma cell lines in vitro. Neuromol Med 2014;16:752–771.
39. De Falco S. The discovery of placental growth factor and its biological activity. Exp Mol Med 2012;44:1–9.
40. Liang J, Piao Y, Henry V, Tiao N, de Groot JF. Interferon-regulatory factor-1 (IRF1) regulates bevacizumab induced autophagy. Oncotarget 2015;6:31479–92.
41. Preston JE, Joan Abbott N, Begley DJ. Transcytosis of macromolecules at the blood-brain barrier. Adv Pharmacol 2014;71:147–63.
42. Gurbaxani B, Dostalek M, Gardner I. Are endosomal trafficking parameters better targets for improving mAb pharmacokinetics than FcRn binding affinity? Mol Immunol 2013;56:660–74.
43. Deissler HL, Deissler H, Lang GE. Actions of bevacizumab and ranibizumab on microvascular retinal endothelial cells: similarities and differences. Br J Ophthalmol 2012;96:1023–8.
44. Mohapatra B, Ahmad G, Nadeau S, Zutshi N, An W, Scheffe S, et al. Protein tyrosine kinase regulation by ubiquitination: critical roles of Cbl-family ubiquitin ligases. Biochim Biophys Acta 2013;1833:122–39.
45. Lampugnani MG, Orsenigo F, Gagliani MC, Tacchetti C, Dejana E. Vascular endothelial cadherin controls VEGFR-2 internalization and

signaling from intracellular compartments. J Cell Biol 2006;174: 593–604.
46. Boucrot E, Ferreira AP, Almeida-Souza L, Debard S, Vallis Y, Howard G, et al. Endophilin marks and controls a clathrin-independent endocytic pathway. Nature 2015;517:460–5.
47. Liu WM, Huang P, Kar N, Burgett M, Muller-Greven G, Nowacki AS, et al. Lyn facilitates glioblastoma cell survival under conditions of nutrient deprivation by promoting autophagy. PLoS One 2013;8: e70804.
48. Hu YL, DeLay M, Jahangiri A, Molinaro AM, Rose SD, Carbonell WS, et al. Hypoxia-induced autophagy promotes tumor cell survival and adaptation to antiangiogenic treatment in glioblastoma. Cancer Res 2012;72:1773–83.
49. Berger C, Madshus IH, Stang E. Cetuximab in combination with anti-human IgG antibodies efficiently down-regulates the EGF receptor by macropinocytosis. Exp Cell Res 2012;318:2578–91.
50. Kuang R, Jahangiri A, Mascharak S, Nguyen A, Chandra A, Flanigan PM, et al. GLUT3 upregulation promotes metabolic reprogramming associated with antiangiogenic therapy resistance. JCI Insight 2017;2:e88815.